Journal of Energy Storage 94 (2024) 112419

Contents lists available at ScienceDirect

Journal of Energy Storage

journal homepage: www.elsevier.com/locate/est

Research papers

Experimental heating and cooling curves of the ground for temporary energy storage applications

Andrés Meana-Fernández [a,*], María José Suárez-López [a], Eduardo Blanco [b], Jesús-Ignacio Prieto [c], David García [a]

[a] Thermal Machines and Engines Area, Department of Energy, University of Oviedo, C/Wifredo Ricart s/n, Gijón, Asturias, 33204, Spain
[b] Fluid Mechanics Area, Department of Energy, University of Oviedo, C/Wifredo Ricart s/n, Gijón, Asturias, 33204, Spain
[c] Applied Physics Area, Department of Physics, University of Oviedo, C/Federico García Lorca s/n, Oviedo, Asturias, 33007, Spain

ARTICLE INFO

Keywords:
Thermal energy storage
Thermal reservoir
Energy supply
Temporary energy accumulator
Experimental testing

ABSTRACT

The building sector represents around 36% of global energy consumption and 39% of atmospheric emissions. Renewable energies require energy storage systems to adjust the gap between energy generation and demand. In this work, an exploratory study of heating and cooling curves of the ground with the aim of evaluating its suitability for temporary energy storage has been performed. Experiments were conducted at three different year periods by injecting heat into a circuit of vertical pipes buried in the ground and then leaving the system evolve on its own, whilst registering the temperature evolution of probes at 5 different depths. The analysis of the dimensionless experimental data revealed a certain asymmetry in the behavior during heat injection and heat dissipation process. During heat injection, the main driving mechanism is the heat power source coming from the water flowing through the buried pipes; whereas during heat dissipation, it is the particular characteristics of the ground. The influence of the water table level was determining, separating an upper and lower zone with a slower and faster response respectively. It was also possible to detect the presence of an underground water stream, that led to convection effects and the removal of heat due to mass transfer, as well as to obtain estimates of the apparent thermal diffusivity of each ground layer. The influence of the year period and atmospheric conditions was especially noticed at the upper ground layers. Accumulated rain beneath the ground and the relative amount of water carried by the underground stream also affected ground thermal properties. Finally, guidelines for the design and placement of heat storage systems based on the results of the study are provided.

1. Introduction

Globally, around 50% of final energy consumption is used for heating purposes, accounting for 40% of CO_2 emissions [1]. The building sector represents around 36% of global energy consumption and 39% of atmospheric emissions [2]. In addition, building stock is expected to increase by 60% for 2050 [3]. The most important mismatch between thermal energy demand and supply is due to the hourly differences between generation and consumption, the variation in the energy cost depending on the time of the day and the distance between generation and consumption sites [4]. In this context, thermal energy storage (TES) systems provide economic and environmental benefits, as they reduce the need of burning fuel. Arce et al. [5] estimated that integration of TES may lead to potential energy savings of 7.5% in Europe, reducing associated gas emissions by 5.5%. Moreover, in Spain, this energy saving potential represents around 20% from the total value of the UE, as it is the country with the highest number of concentrated solar power plants. Hence, an accumulation system can contribute to match the gap between energy production and demand [6]. Currently, energy storage is performed mainly by compressed air, batteries, hot or cold water, ice or inertial batteries [7]. Plenty of research on hydrogen possibilities has been performed, due to its potential versatility for final uses, but its production and storage are generally more expensive, considering its low volumetric energy density.

TES systems may be applied to standalone buildings, multiple building systems, districts and urban networks with a wide range of applications [8]. Some of their benefits are: reduction of heating and cooling energy demand, integration of clean energy sources, increase

* Corresponding author.
E-mail address: andresmf@uniovi.es (A. Meana-Fernández).

https://doi.org/10.1016/j.est.2024.112419
Received 30 November 2023; Received in revised form 31 March 2024; Accepted 31 May 2024
Available online 10 June 2024

Nomenclature

Greek symbols

α	thermal diffusivity, m^2/s
Π_x	dimensional group associated to property x
ρ	density, kg/m^3

Roman symbols

c	specific heat capacity, J/(kg K)
D	tube diameter, m
d	distance from tube center to probes, m
Fo	Fourier number
k	thermal conductivity, W/(m K)
L	tube length
r	radial distance to tube center, m
T	temperature, °C
t	time, s
z	depth, m

Subscripts and superscripts

0	initial property
∞	steady ground property
a	apparent property
ref	reference property

of generation capacity and flexibility of energy systems, reduction of emissions and increase of energy efficiency, waste heat recovery, and increase of operational life and cost reduction in roads, pavements and bridges by dampening extreme temperature changes. When the energy to be stored is of low thermal potential, TES may reach process global efficiencies between 50 and 100% [4], becoming the most adequate technology for heat storage in concentrated solar plants or nuclear reactors [9]. The waste heat energy potential in the EU has been estimated as 300 TWh per year [10], and great part of this heat could be stored in the warmer periods to be later used in the colder ones [11]. Thermal energy may be stored as sensible or latent heat, as thermochemical energy, or as a combination of the three [12]. Apart from integrating renewable sources by balancing the gap between energy generation and demand, thermal systems may be improved by introducing TES. These systems do not suffer the degradation caused by the loading and unloading cycles, as batteries, they present more convenient life cycles and a longer useful life, and the materials used are less toxic [4]. The most commonly used heat sources, storage temperatures, efficiencies and uses for stored heat have been summarized in [11], as well as the benefits and drawbacks of each technology. A TES system may be described as a function of the following characteristics [13]: energy storage capacity, loading and unloading speed, or system power, efficiency or ratio between loaded and recovered energy, storage period (days, weeks, months), loading and unloading times, investment and operational costs (per unit capacity or power), and useful life (number of loading and unloading cycles).

Natural materials arise as a sustainable option for heat storage. Rocks, sand or gravel are economic, easy to obtain, non-toxic or flammable, and they may act as heat transfer surfaces and storage systems at the same time [4]. For instance, with high-porosity and permeability rocks saturated with water, the water could be used to drive heat from the surface to the storage system and vice-versa [14]. Due to the stability of ground temperature during the year in comparison with atmospheric temperature, it becomes an interesting option for heating and cooling applications in buildings. This stored energy may be used directly or coupled with heat pumps [15]. In such developed facilities, it is easy to store surplus energy from renewable sources, as in solar thermal plants [16,17]. Considering the type of thermal system, borehole TES (BTES) has a great popularity, due to its economic cost and the lower requirements for its installation [17]. In borehole installations, a closed loop with pipes inserted in wells working as heat exchangers allows to access the vast capacity of the underground to store sensible heat [18]. There is a heat source, the well storage, the heat exchangers, and usually a support tank due to the typically slow loading and unloading speeds [19]. The pipes may be vertical and U-shaped, placed with spacing in the storage field and with depths from 20 to 200 m [20], or horizontally buried in trenches. Insulation may be added on the ground surface [21]. Regarding the characteristics of the ground, Alva et al. [4] claim a high specific heat, a high thermal conductivity and low hydraulic conductivity are desired properties, trying to reduce the underground heat flux.

Although many initial BTES projects stored heat in summer for heating purposes in winter, they may be also used as cold storage systems if the underground is cooled by using atmospheric air as a heat sink in winter. This is a high-efficiency technique that consumes very few electricity during operation [21]. Nevertheless, the most popular use is a combined system that stores heat and cold, so the underground works as a heat source at low temperature in winter, coupled to a heat pump, and works in direct cooling mode in summer, activating the heat pump only when the thermal reserve is depleted. The system could be also used to reduce the cooling power installed and allow a more continuous operation of the cooling equipment [22]. On the other hand, underground sensible heat storage may be used to store heat or cold when electricity price is low and use it when it rises up. Several studies have shown promising results, from the installation of TES systems beneath building foundations [6], to the use of sand beds in both cold [23] and hot [24] climates. With subterranean water, it was possible to cover up to 98% of heating demand in cold climates [25]. Compared to aerothermal systems, a reduction of 74% of electricity demand was found by Lu, He & Mao [26]. After verifying the impossibility of transitioning directly to a low-temperature solar energy urban heating system for the university of Darmstadt, Formhals et al. [27] proposed a step-by-step transition by reducing the net temperatures successively. To this aim, they supported the transition with an underground thermal storage system. Other example of underground heat storage at large scale may be found in [28], who evaluated the possibility of coupling it with Power-to-X systems. Finally, since the 4th generation of urban district heating systems (DHS), network temperatures are becoming lower, using heat generated from renewable sources or industrial waste heat [29]. Therefore, TES systems are becoming increasingly relevant for the design of smart cities.

The need of developing and implementing intelligent and flexible thermal systems that integrate thermal energy storage is clear [6]. In the experimental field, ASHRAE standards can be used for testing TES systems (943 - Method of Testing Active Sensible TES Devices Based on Thermal Performance and 94.1-1985 - Method of Testing Active Latent Heat Storage Devices Based on Thermal Performance). To determine the effective thermal conductivity and the thermal resistance of boreholes, the so-called Thermal Response Test may be used [30]. This test injects a heat pulse through a fluid inside the well, allowing to obtain the thermal response from the average of the inlet and outlet fluid temperatures. Coupling the results with an approximate model of underground heat transfer and considering the ground as homogeneous and isotropic, neglecting geological layers of underground water, it is possible to obtain approximations of the ground thermal conductivity and the thermal resistance with errors around 5% and 10% [21]. Complementarily, measuring the temperature profile along the borehole depth may provide valuable information about the geological layers and potential underground water streams (VDI Guideline 4640) [31].

One of the research lines identified by Dincer and Rosen [7] is the study of operating conditions and efficiency of TES related to energy conservation in buildings, including heat and mass transfer in

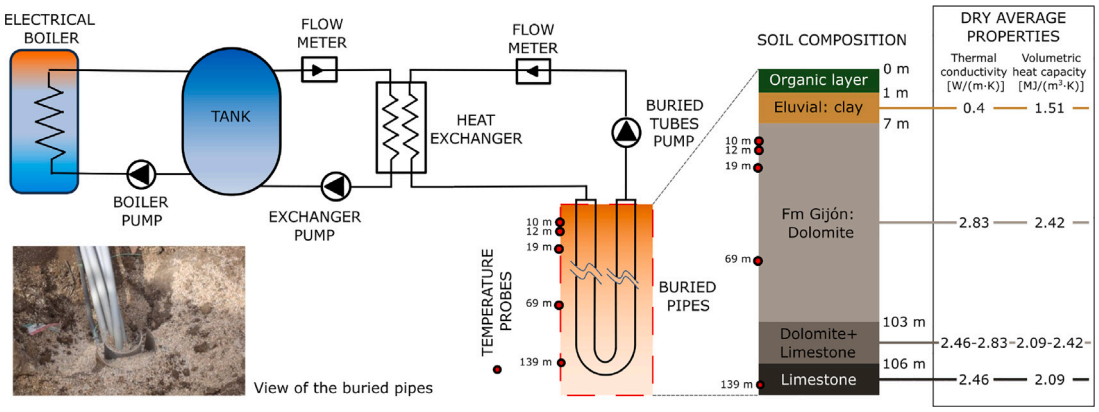

Fig. 1. Scheme of the vertical pipes circuit alongside the geological description and a view of the buried pipes entering the ground.

transient conditions, so that electricity demand may be changed to periods in which it is more economic. The application of solar heating and factors that affect TES are also potential research ideas. Two of the main barriers for adopting TES systems, following [7], are the lack of adequate information and commercial options, and the lack of demonstrations of local long-term TES systems such as aquifers or boreholes. Considering that the development of knowledge about the working principles of TES in borehole systems, setting the focus on local technologies, and the realization of R&D activities in TES systems may help to contribute to advancing the development of commercial systems, in this experimental work, the behavior of the ground as a temporary energy accumulator is studied.

In the 2000s, 5 office building prototypes were built or retrofitted in the context of the strategic project ARFRISOL [32]. The main objective of this project was to show the adequacy of bio-climatic architecture and solar energy integration in buildings, considering both heating and cooling, as well as electricity production. Thanks to that project, the Gijón Solar Cooling Laboratory (GSCL) [33] was installed at the University of Oviedo. This laboratory allows testing different heating and cooling technologies in a modular arrangement, including a geothermal installation with vertical buried pipes. With funding from the project RehabilitaGeoSol [34], it was possible to complete the experimental facility, obtaining the first results from the circuit of vertical pipes. This work, completing the results presented in [35], presents experimental results from the heat loading and dissipation curves in the vertical buried pipes of the laboratory, providing insight into the influence of depth and the year period on the thermal behavior of the ground.

2. Materials and methods

2.1. Geology of the area and experimental facility

The idea behind the inception of the GSCL was the possibility of testing diverse solar cooling technologies for buildings. The facility is located in the Polytechnical School of Engineering of Gijón from the University of Oviedo and is based on a lithium chloride absorption machine ClimateWell-CW10 which may be connected to different heat sources or sinks. In addition, the machine has two different barrels to mix LiCl and water, being possible to charge one barrel while discharging the other one. Heat may be generated in a solar collector, a biomass boiler or an electrical boiler, whereas heat dissipation may be performed in a dry cooler, a water cooling tower, a water reservoir or a series of ground heat exchangers consisting of vertical and horizontal pipes. In Fig. 1, a scheme of the equipment from the facility used in this work is shown: the electrical boiler, a hot water storage tank, a heat exchanger and the set of vertical buried pipes, alongside the circulation pumps and the instrumentation (flowmeters and temperature probes). The figure also contains a graphical description of the geology of the area, as well as a view of the buried pipes. The ground, as shown in the scheme on the right side of Fig. 1, is composed of a superficial organic layer with 1 m of depth. Afterwards, an eluvial layer consisting of clay extends down to 7 m deep. Then, the formation corresponding to Gijón location, composed of dolomite, encompasses depths from 7 to 103 m below the ground, mixing with limestone at depths from 103 to 106 m. From this depth on, the soil is mainly composed of limestone. The thermal characteristics measured from a series of dry-ground probes may be found next to the description of the geology, i.e., thermal conductivity and volumetric heat capacity. Note that the values correspond to dry ground average properties.

The experiments proceeded as follows. Firstly, the electrical boiler was used to heat water, which was then circulated to a hot water storage tank. Then, via a heat exchanger, heat was transferred to a closed-loop circuit of vertical pipes that are buried into a 140 mm diameter borehole in the ground, filled with gravel. Each loop consists of 2 U-shaped circuits with 32 mm diameter pipes, reaching a maximum depth of 140 m. A detailed view of the constructive characteristics of the pipes inside a borehole is depicted at the bottom-left part of Fig. 1. The instrumentation used to monitor the heat injection and dissipation processes is the following: five 3-wired PT-100 probes fitted to the outer pipe surface at depths of 10, 12, 19, 69 and 139 m; and two Kobold inductive flowmeters, one for the tank-heat exchanger circuit and other for the buried pipes-heat exchanger circuit. This instrumentation was wired to a Keithley 2700 multimeter, coupled to a multiplexer 7700 that allowed the connection to a PC, recording data every five minutes. The accuracy of the PT-100 probes is ±0.15°C, while the accuracy of the flowmeters is ±0.3% of the measurement.

2.2. Experimental tests

The experimental tests sought to gather data about the thermal response of the ground at different months of the year, so three periods, corresponding to winter, spring and late summer in the region were selected. The first measurement campaign was performed in May 2019, followed by September 2019 and February 2020. Fig. 2 shows an example of the experimental curves obtained in May 2019. As it may be observed, the tests consist of two stages: heat injection and heat dissipation. During the heat injection stage, hot water from the storage tank is driven through the geothermal circuit until stationary conditions are measured at the temperature sensors. Afterwards, the circuit is stopped and the dissipation of heat is monitored. During all the process, the temperature at all probe positions from 10 to 139 m depth is measured. Table 1 collects the main global conditions of the experimental tests: heat injection time, average temperature, flowrate and average injection power, heat dissipation monitoring time, and total experiment time. The different conditions regarding heat injection were selected trying to keep similar heating power values between

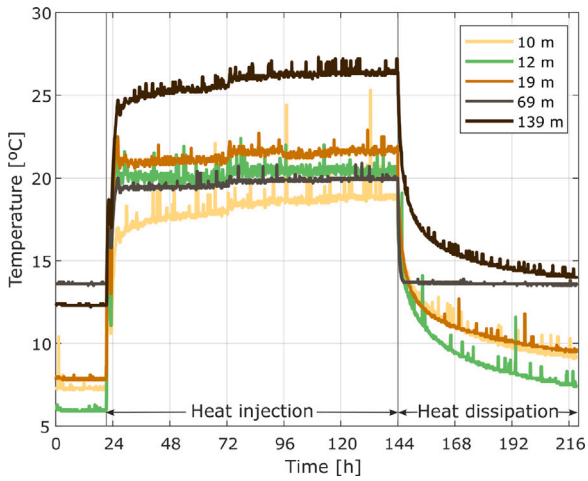

Fig. 2. Temperature evolution at different depths during the experiments of May 2019.

Table 1
Summary of experimental test conditions.

	May	September	February
Heat injection time	8,685 min	20,000 min	10,110 min
Average heat injection temperature	44.7 °C	43.0 °C	47.3 °C
Heat injection flowrate	19.2 L/min	22.5 L/min	11.6 L/min
Average heat injection power	17.5 kW	15.5 kW	14.0 kW
Heat dissipation monitoring time	4,515 min	19,315 min	21,690 min
Total experiment time	13,200 min	39,315 min	31,800 min

the experimental campaigns to allow the comparison between different periods, although using different temperature and flowrate values. The total experiment time was determined by the maximum period without interruptions in electric supply.

2.3. Dimensional analysis

Before analyzing the experimental results, dimensional analysis was applied to the problem. As considered by Reuß [21], for the first approximation, the ground thermal conductivity was assumed to be isotropic. The temperature and characteristic ground properties are assumed to be scalar functions and have cylindrical symmetry. The ground surface was assumed to be adiabatic to perform the dimensional analysis, awaiting the later evaluation of the effect of atmospheric conditions. Following the procedure detailed in [35], a relationship for the temperature difference ΔT between a point below the ground at depth z and a distance r from the pipes, and a point located at the same depth and away from the influence of the pipes may be obtained as:

$$\Delta T = f(r, z, D, L, k, \rho, c, \Delta T_0, t) \tag{1}$$

where D and L are the pipe diameter and length in m; k, ρ and c are the thermal conductivity in W/(m K), the density in kg/m^3 and the specific heat capacity in J/(kg K) of the ground; ΔT_0 is the temperature difference at the start of the heat dissipation process in K, and t is the elapsed time in s. After applying Buckingham's Pi theorem, the following functional relationship between dimensionless groups is obtained:

$$\frac{\Delta T}{\Delta T_0} = F\left(\frac{r}{L}, \frac{z}{L}, \frac{D}{L}, Fo, \Pi_t\right) \tag{2}$$

where $Fo = \alpha t / L^2$ is the Fourier number and $\Pi_t = \Delta T_0^{1/2} c^{1/2} t / L$. This result, obtained by means of the classic dimensional analysis, considers the variables as scalars. Nevertheless, considering the algebraic nature of the variables, spatially discriminated dimensional analysis can be applied, with the advantage of reducing the final number of dimensionless variables involved in the problem [35]. Through this analysis, it can be detected that the monomial Π_t may be left out of the list of influencing monomials, as it is not neither justified experimentally nor found in similar problems in the literature. In addition, as r, D and L have constant values in the present case study, a simplified functional relationship can be used for the present experimental study:

$$\frac{\Delta T}{\Delta T_0} = F\left(\frac{z}{L}, Fo\right) \tag{3}$$

2.4. Postprocessing of results

Firstly, a third-order one-dimensional median filter was applied to the measurements [36] to remove outliers. After that, results were made dimensionless to allow for the comparison of different depths and year periods.

The exact evolution of ground thermophysical properties is not known, so a constant and isotropic value for the apparent thermal diffusivity $\alpha_{ref} = 5.288 \cdot 10^{-7}$ m^2/s was used to make variables dimensionless, consistent with the trial pit values from the RehabilitaGeosol project [34] for density, 3200 kg/m^3; specific heat, 1300 J/(kg K); and thermal conductivity, 2.2 W/(m K). However, due to the observed different behaviors at different depths, as depicted in Fig. 2, an attempt was made to obtain an estimate for each ground depth. With this objective, the apparent thermal diffusivity α_a was left free for each data series, obtaining estimated values from the fitting of the experimental results, using the equation proposed in [37] for transient heat conduction in semi-infinite solids:

$$\Delta T(t) = \Delta T_0 \operatorname{erf}\left(d / \sqrt{4\alpha_a t}\right) \tag{4}$$

Here, d is the distance between the tube center and the probe position, 0.07 m. Values of α_a in the order of magnitude of 10^{-7} are to be expected, in line with typical values reported in the literature [38–40].

2.5. Atmospheric weather effects

Atmospheric conditions, especially, temperature and humidity, may influence the behavior of the uppermost ground layers. To provide explanations for different behaviors at different year periods, meteorological data corresponding to the days in which the experiments were performed, up to the previous month, were collected from the Spanish State Agency for Meteorology AEMET [41]. The results have been collected in Table 2, with the hope of providing insight into the understanding of weather effects in the boundary conditions that affect the ground thermal behavior.

Regarding temperature records, average atmospheric temperatures are 12.4 °C, 18.4 °C, and 10.7 °C for the experiments of May 2019, September 2019 and February 2020 respectively. Comparing injection and dissipation, May showed an increasing trend in temperatures; whereas September showed a decreasing trend. In the case of February, average temperatures decreased slightly. Considering precipitations, a high period of rain before the start of the experiments may be found in May 2019, with 91.9 mm, followed by February 2020, with 49.2 mm, while September 2020 was the driest month, with 29.2 mm. These trends changed during the experiments, with May 2019 being the driest, with 5.2 mm. September 2019 was wetter, with 11.2 mm, whilst February was the wettest month, with 19.2 mm. Comparing heat injection and dissipation periods, just 1 mm was found in May for injection, followed by February with 5.2 mm, and a relatively high amount of rain was found in September, 10.4 mm. On the other hand, during dissipation, almost no rain (0.8 mm) was found in September, 4.2 mm were found in May, and 14 mm were found in February. Temperature affects heat capacity and thermal conductivity, both typically increasing with temperature, so that the changes in thermal diffusivity will be linked to the relative change of these two variables. In addition, it has been verified that the different ground constituent minerals and rocks

Table 2
Weather atmospheric conditions at the experiment dates.

	May	September	February
Cumulative precipitation (1 month before experiments)	91.9 mm	29.2 mm	49.2 mm
Cumulative precipitation (1 week before experiments)	15.4 mm	6.2 mm	11.0 mm
Average ambient temperature during injection	11.4 °C	18.8 °C	10.9 °C
Cumulative precipitation during injection	1 mm	10.4 mm	5.2 mm
Average ambient temperature during dissipation	14.5 °C	17.2 °C	10.6 °C
Cumulative precipitation during dissipation	4.2 mm	0.8 mm	14 mm

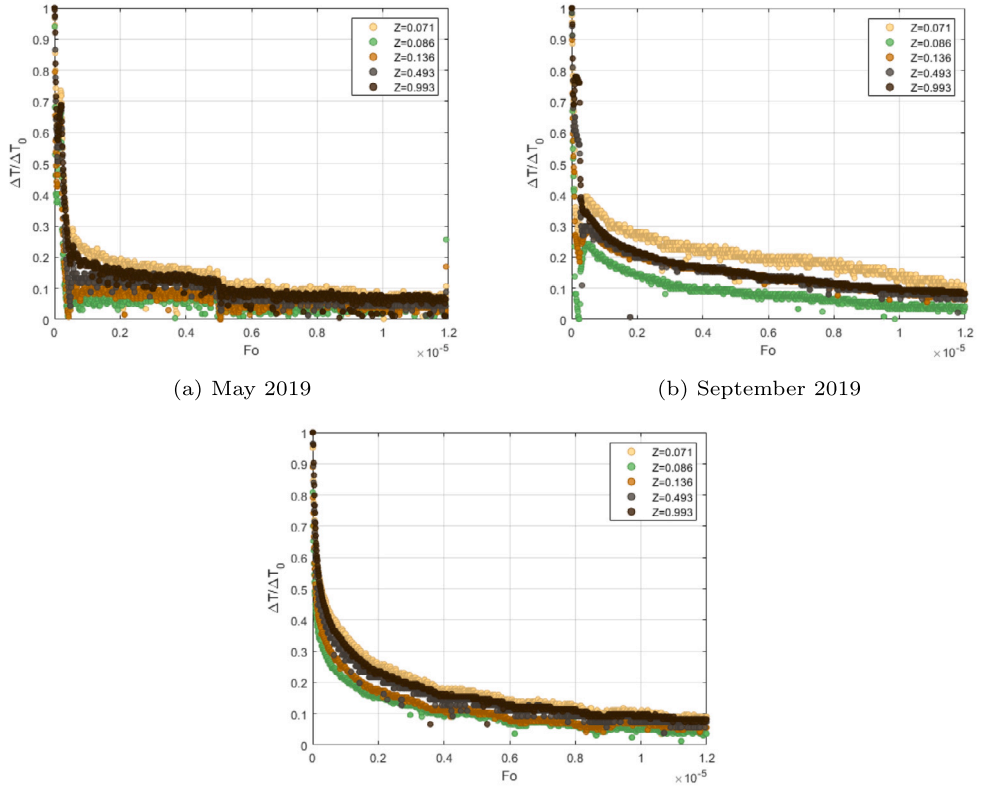

(a) May 2019 (b) September 2019

(c) February 2020

Fig. 3. Dimensionless heat injection curves in different periods (constant ground diffusivity).

typically leave gaps in between, that may be filled with fluids [42]. The heterogeneous composition of the ground represents a difficulty for estimating its thermophysical properties, with an increase in humidity linked to an increase in thermal conductivity and volumetric heat capacity [43]. Nevertheless, with increasing levels of water, ground thermal conductivity reaches a maximum, whereas the heat capacity continues to increase. Therefore, for ground thermal diffusivity, an increasing tendency with humidity is expected, reaching a maximum, and decreasing afterwards [44,45].

3. Results and discussion

At a first glance, there was no observable effect of atmospheric temperature oscillations, even at the probes at the shallowest ground layers, in any of the studied periods. In this section, firstly, the effects of ground depth considering a constant thermal diffusivity will be presented and discussed. Then, these effects will be reviewed, but allowing for the vertical variation of the ground thermal diffusivity.

3.1. Effects of ground depth considering constant ground thermal diffusivity

Results for heat injection and dissipation, considering a constant ground thermal diffusivity, are presented in Figs. 3 and 4.

Regarding the heat injection curves in Fig. 3, the ones from May seem to evolve faster. Although this effect could be related to the higher average heat injection power (around 12.9% higher than in September), must have another explanation, because the curves from September, which had a higher average heat injection power than the ones from February (around 10.7%), evolve slower. Looking at Table 2, it could be argued that the fastest curves are related to the period with more accumulated precipitation before the heat injection stage (May - Fig. 3(a)), whereas the slowest ones happened in the period with the lowest amount of precipitations (September - Fig. 3(b)). The water retained in the gaps between the ground constituents could be related to an increase in the thermal conductivity, increasing its thermal diffusivity. The apparent shift due to depth in the curves from September in comparison with other months is related to the x – temporal – axis, which becomes enlarged due to the longer time required to reach steady-state conditions. Nevertheless, considering the variations related to depth in the three periods, it may be observed that the slowest evolving curve is the uppermost one (Z = 0.071). Probably, the proximity to a colder ground level is the responsible of this behavior. Surprisingly, the deepest regions evolve at a slower speed than the region at Z = 0.086. This fact could be related to the depth at which the water table is located (15 m below ground level, corresponding to Z = 0.107). Being these layers saturated with water, probably the maximum of thermal conductivity has been reached,

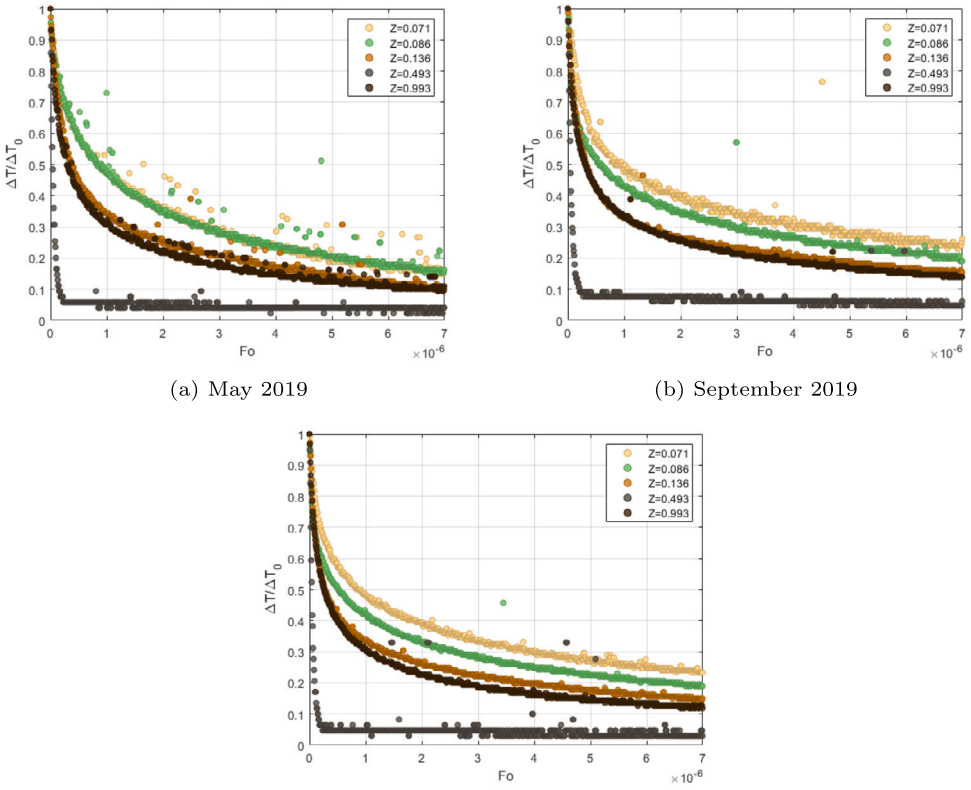

(a) May 2019 (b) September 2019

(c) February 2020

Fig. 4. Dimensionless heat dissipation curves in different periods (constant ground diffusivity).

whilst the heat capacity and density have continued to increase, thus decreasing thermal diffusivity.

Comparing the heat dissipation curves shown in Fig. 4 with the previous ones from Fig. 3, a certain asymmetry in the behaviors at heat injection and dissipation may be appreciated. The effect of depth is not so determining at heat injection as it is at heat dissipation, hinting at some kind of "ground thermal asymmetry". It seems that, due to the vicinity of the sensors to the water circulating inside the pipes, once the heat source is removed and the system is left to evolve on its own, the particular characteristics of each ground layer become more appreciable.

By looking at Fig. 4, an upper zone corresponding to $Z \leq 0.086$ shows evolution trends different to the ones in the lower zone ($Z \leq 0.136$). This result agrees with the heat injection behavior, considering that the water table divides the ground into two distinct regions. On the other hand, the abrupt behavior of the curve at $Z = 0.493$ shows that the ground is incapable of keeping the heat stored at this depth for as long as at the other depths. This rapid decrease of temperatures during dissipation must be explained by a different heat transfer mechanism, such as an underground water stream, able to extract heat at a higher rate thanks to the continuous renewal of water and the additional convection mechanism. Finally, comparing the three months, the gap size between upper and lower ground regions is larger in May than in the other months. A possible explanation is the less amount of rain before the heat dissipation stage, so, when it rains then, it contributes to lower the temperature of the upper layers of the ground and increases their thermal conductivity. In addition, in September and February, there was more rain during the heat injection process, which could have increased ground heat capacity, and consequently, the injection time required to reach steady conditions and the thermal energy stored before initiating heat dissipation. The region below the water table, nevertheless, does not appear to be so affected by the weather.

3.2. *Effects of ground depth considering vertical variation of ground thermal diffusivity*

After comparing the heat injection and dissipation trends, the possible vertical variation of ground thermal diffusivity was considered by fitting the experimental data with Eq. (4). Regarding heat injection curves, when the variables were made dimensionless, temperature evolution seems to collapse into the same trend for all depths, as shown in Fig. 5.

This suggests that the dominant heat transfer mechanism is the same at all depths: the heat power source coming from the water inside the pipes. Convection will make the inner tube wall reach a temperature close to the circulating water relatively soon, transferring afterwards heat by conduction to the outer walls of the pipes and the surrounding ground. The heat injection in the first tests (Fig. 5(a)) shows an initial oscillating pattern, caused by the electric boiler control system.

Estimates of apparent thermal diffusivity values for each ground layer obtained from the temperature data fitting for the different year periods tested are shown in Fig. 6, and actual values have been collected in Table 3.

Although the range of thermal diffusivity values for the ground may be very broad, the results are similar for all depths and months, ranging from 3 to $8 \cdot 10^{-7}$ m^2/s, in the order of magnitude of the values reported in the literature (10^{-7} m^2/s). In addition, it has been observed how values stabilize below the water table, from $Z = 0.136$ down, for all months, whereas values above the water table are more affected by ambient conditions. A possible explanation for the slightly

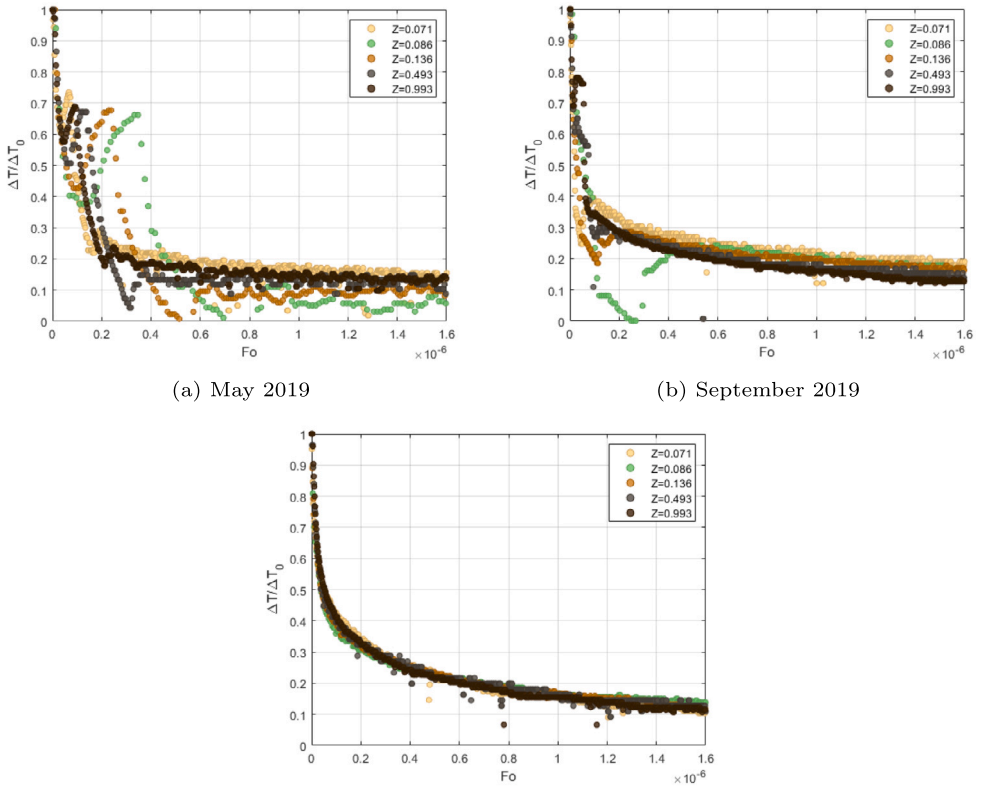

(a) May 2019

(b) September 2019

(c) February 2020

Fig. 5. Dimensionless heat injection curves in different periods (different layer diffusivity).

Table 3
Apparent ground thermal diffusivity as a function of dimensionless depth and period.

$Z = z/L$	May $\alpha \times 10^7$ [m^2/s]	September $\alpha \times 10^7$ [m^2/s]	February $\alpha \times 10^7$ [m^2/s]
0.071	5.69	3.38	3.99
0.086	7.77	5.58	7.26
0.136	3.75	3.95	4.77
0.493	5.88	6.03	6.03
0.993	4.77	4.72	4.61

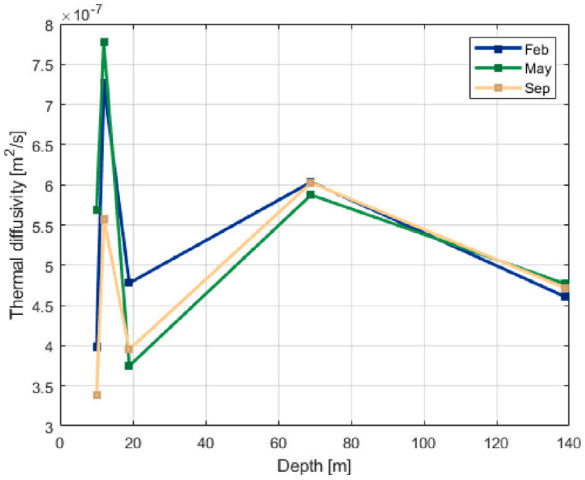

Fig. 6. Apparent thermal diffusivity as a function of depth for different months.

higher values found at the upper ground layers in May could be, indeed, the higher amount of precipitation. Values below the water table ($Z = 0.107$) seem to be more stable all year round, hinting at the possibility of a more stable storage system at these depths. Diffusivity changes at the layers above the water table may be ascribed to weather effects and will be commented in the subsequent subsection. Finally, the relatively high diffusivity values for the heat injection stage in May can be related to the amount of rain registered up to one week before the experiment. The accumulation of water, coupled to the higher heat injection power, could have caused the oscillating response from the system up to $Fo = 0.5$ in Fig. 5(a). Therefore, the exact values of diffusivity obtained from the fitting of data, although valuable for the comparative analysis, should be considered with care.

On the other hand, once the heat injection stage is finished, the power source is removed and the system is left free to evolve, a heat transfer mechanism hidden until that moment is revealed: all curves collapse into the same one, apart from the one located at $Z = 0.493$, which shows a totally different trend, as depicted in Fig. 7.

This particular depth is thought to be related to an underground water stream, which allows a higher heat dissipation rate by convection and the constant renewal of cold water. Hence, dimensionless representations with different thermal diffusivity values for each ground layer may be useful to identify the dominant heat transfer mechanism. In addition, they also confirm the physical explanation for the differences observed in heat injection and dissipation processes from Figs. 3 and 4 at that depth. During heat injection, the dominant heat transfer process is related to the continuous supply of hot water to the pipes, with all curves exhibiting similar trends. During heat dissipation, the main heat transfer mechanism is dissipation beneath the ground towards colder regions. In the case of the ground, the dominant mechanism is conduction; but, when underground water currents are present, convection and water mass transfer acquire a more dominating role in heat transfer.

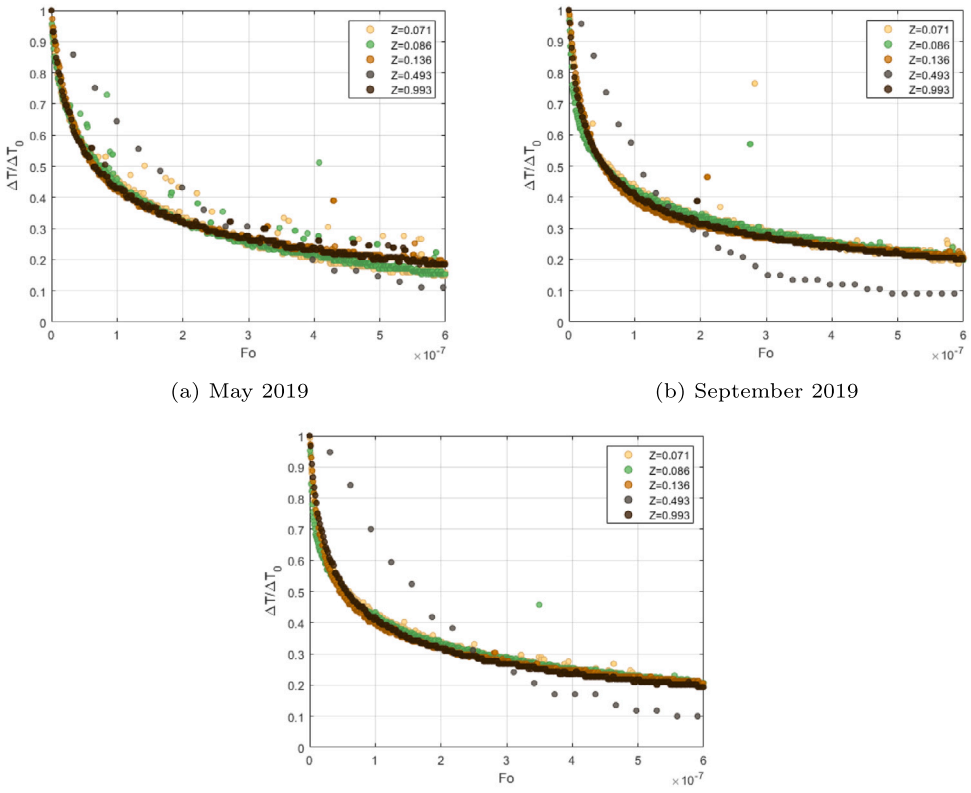

(a) May 2019

(b) September 2019

(c) February 2020

Fig. 7. Dimensionless heat dissipation curves in different periods (different layer diffusivity).

3.3. Seasonal and atmospheric effects

To evaluate the differences between the system behavior at different year periods, Figs. 8 and 9 are presented for heat injection and dissipation stages.

Regarding the heat injection curves depicted in Fig. 8, it must be noted that, as different injection conditions were used, a detailed comparative quantitative analysis is out of scope. However, it is possible to perform a qualitative comparison between the temperature evolution for different months. The trends of the curves are similar, especially from $Fo = 2.5{\cdot}10^{-6}$ up. The differences up to that point may be ascribed to the injection process itself, with the smoother curves from February corresponding to the lowest heat injection flowrate. Instabilities in the electric boiler control system were observed during heat injection in May, which had the highest average heat injection power, being a possible cause for the different behavior with respect to the other months up to $Fo = 2.5 \cdot 10^{-6}$, This issue, coupled to the higher amount of rain registered before beginning the experiments, may explain the different behavior alongside the higher apparent diffusivity values collected in Table 3. With the similarity in the shape of the curves in May and the ones corresponding to the underground water stream found at $Z = 0.493$ for dissipation, it might be argued that, indeed, the ground is relatively wet. This effect is visible at all depths, so it seems that the ground has not been able to drain all the precipitated water from the layers above the water table. Comparing the curves from September and February, they present similar values, except at the uppermost layer (Fig. 8(a)). Considering that February was a colder month and with more rain intensity before starting the experiments, this could explain why the evolution of February curves is faster. With water increasing thermal conductivity, and starting from a lower initial temperature, it seems logical that the curve reaches before smaller values of dimensionless temperature. On the other hand, the higher amount of rain registered during the injection stage in September could have influenced the loading process by lowering the temperature of the uppermost ground layer, shifting the curve upwards.

When the evolution of dimensionless temperatures at heat dissipation was observed, as in Fig. 9, almost no differences were found between the curves. Curves from February and September follow almost the same pattern, with small differences being probably due to the same causes related to weather conditions and rain accumulation already commented with the heat injection results. The curves from May present a similar trend but, at lower depths, the slope of the curves is higher. This behavior may be attributed to a higher level of water accumulated from the rain. Nevertheless, this effect is not so significant as in the heat injection curves from Fig. 8, so most of the accumulated water must have been already drained by the ground. Looking at the effect of the year period for different depths, it seems that the energy stored at the uppermost layers of the ground is more influenced by ambient conditions. Therefore, insulation would required at the upper ground layers, to avoid interference from atmospheric conditions. Finally, the slight difference between the curves for September and the other periods at the lower depths may be attributed to the effects of the underground water stream at $Z = 0.493$. After summer, the stream carries less water, not being able to draw heat at the same rate as in February.

To sum up, it has been observed that the introduction of water into the ground increases thermal conductivity and diffusivity up to a certain limit in which the thermal conductivity reaches its maximum. This allows the design of faster heat injection and recovery curves for energy storage, as in the required experiment times collected in

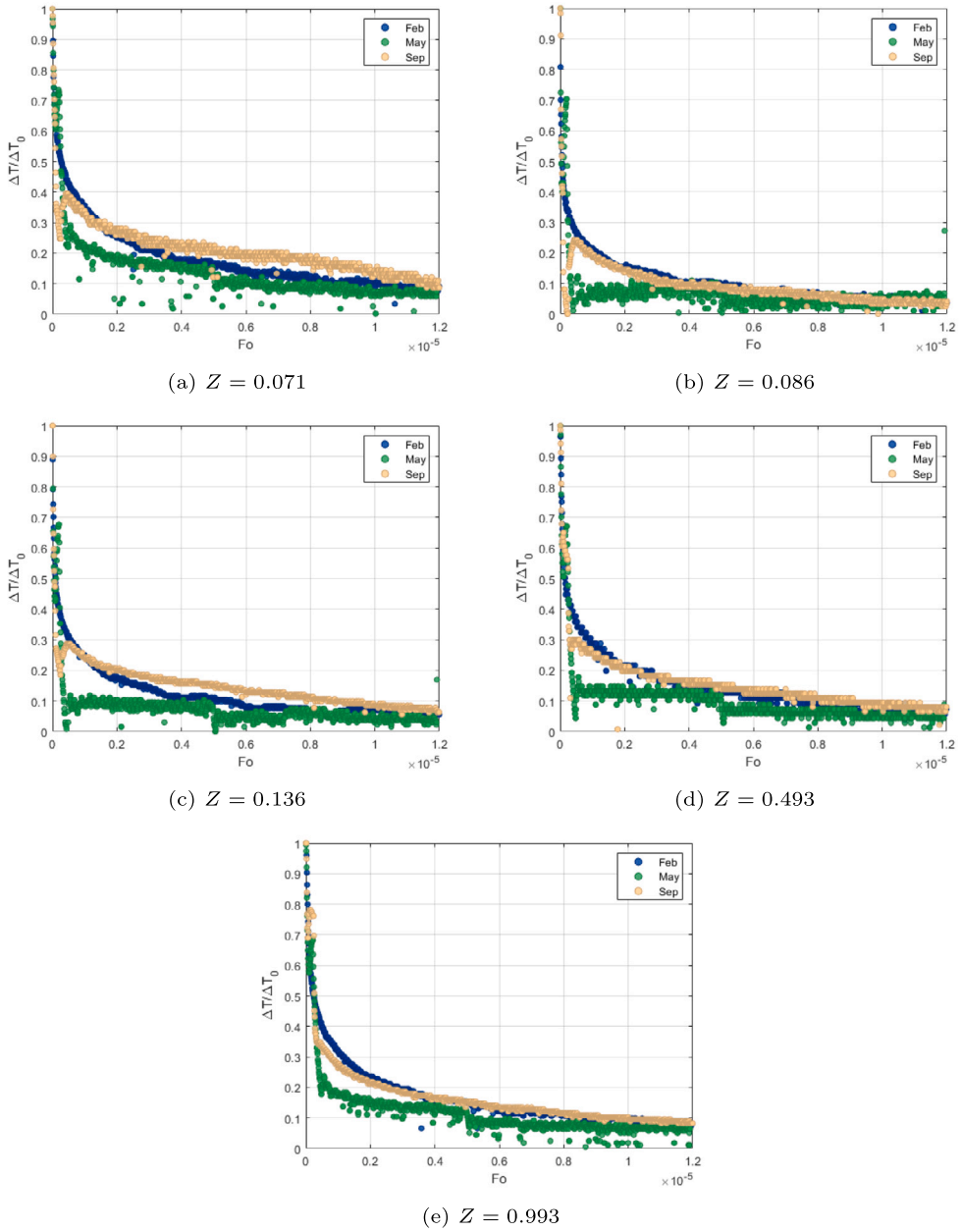

(a) $Z = 0.071$ (b) $Z = 0.086$

(c) $Z = 0.136$ (d) $Z = 0.493$

(e) $Z = 0.993$

Fig. 8. Dimensionless heat loading curves at different depths for different periods.

Table 1 for May. Considering that wet ground has higher specific heat and density, it will represent an advantage for the quick storage and recovery of heat energy with a higher specific energy density, with insulation helping to increase storage times. However, if small heating power values are required, dry ground could store energy for longer times requiring less insulation.

4. Conclusion

The main conclusions of this work may be summarized as follows:

1. The study aims to assess the feasibility of using the ground for temporary energy storage through the analysis of heat injection and dissipation curves.
2. Experimental tests were conducted using vertical buried pipes in the Gijón Solar Cooling Laboratory. Significant asymmetry was observed between heat injection and dissipation processes. The proximity to colder ground levels slowed the temperature evolution during heat injection. The water table level influenced the thermal response, with different evolution speeds above and below. Ground saturation with water increased thermal inertia.
3. During heat dissipation, distinct trends were observed between upper and lower ground regions, influenced by the water table level. Underground water streams contributed to heat dissipation through convection effects. Apparent thermal diffusivity estimates align with literature values, although a qualitative interpretation was emphasized.
4. The findings suggest opportunities for designing faster heat injection and recovery curves with water introduction into the ground. Ground characterization, including the water table level and climate conditions, is crucial for selecting suitable depths

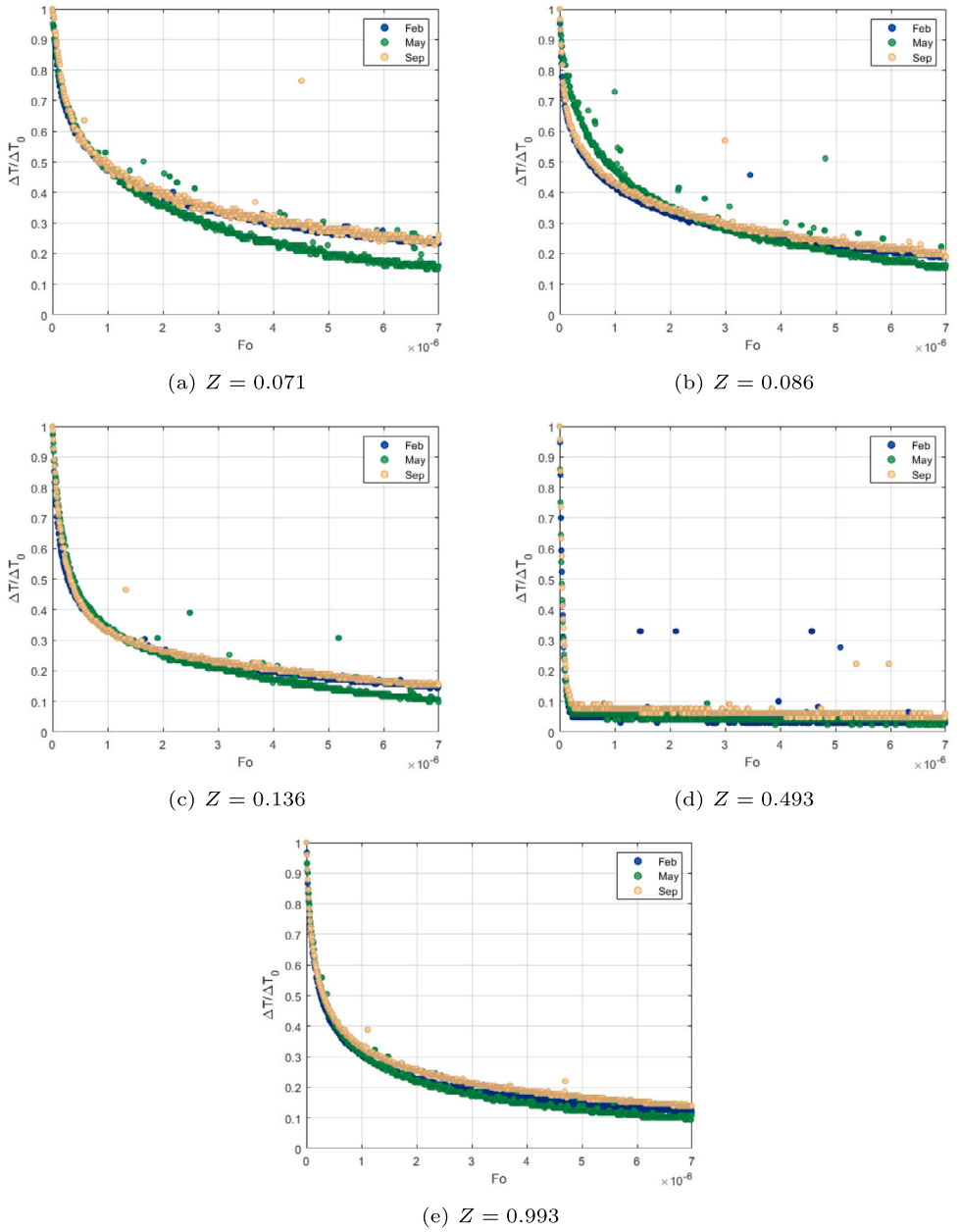

(a) $Z = 0.071$ (b) $Z = 0.086$

(c) $Z = 0.136$ (d) $Z = 0.493$

(e) $Z = 0.993$

Fig. 9. Dimensionless heat dissipation curves at different depths for different periods.

for thermal energy storage. The analysis of heat loading and dissipation curves offers valuable insights into the viability of ground-based energy storage solutions.

CRediT authorship contribution statement

Andrés Meana-Fernández: Data curation, Formal analysis, Investigation, Methodology, Visualization, Writing – original draft. **María José Suárez-López:** Conceptualization, Formal analysis, Investigation, Methodology, Writing – original draft. **Eduardo Blanco:** Conceptualization, Funding acquisition, Investigation, Project administration, Supervision, Writing – review & editing. **Jesús-Ignacio Prieto:** Formal analysis, Funding acquisition, Investigation, Methodology, Project administration, Supervision, Writing – review & editing. **David García:** Writing – original draft, Visualization, Supervision, Methodology, Investigation, Conceptualization, Data curation, Formal analysis.

Declaration of competing interest

The authors declare that they have no known competing financial interests or personal relationships that could have appeared to influence the work reported in this paper.

Data availability

Data will be made available on request.

Acknowledgments

This research was funded by the National Research and Development Plan 2004–2007 (Ref. PS-120000-2005-1), co-financed by ERDF funds and supported by the Spanish Ministry of Science and Innovation.

This research has also been developed in the framework of the REHABILITAGEOSOL (RTC-2016-5004-3) project. It is a multidisciplinary R&D program supported by the Spanish Ministry of Science and Innovation and co-financed by European Regional Development Funds (ERDF). The authors would like to thank the AEMET OpenData system from the Spanish State Agency for Meteorology (AEMET), for making available the meteorological data used in this work.

References

[1] International Energy Agency (IEA), Renewables 2019, 2019, Paris, France. https://www.iea.org/reports/renewables-2019. (Accessed 21 February 2023).
[2] International Energy Agency (IEA), Global status report for buildings and construction 2019, 2019, Paris, France. https://www.iea.org/reports/global-status-report-for-buildings-and-construction-2019. (Accessed 21 February 2023).
[3] M. Swilling, B. Robinson, S. Marvin, M. Hodson, M. Hajer, City-level decoupling: urban resource flows and the governance of infrastructure transitions. a report of the working group on cities of the international resource panel 2013, 2013, https://www.resourcepanel.org/reports/city-level-decoupling. (Accessed 21 February 2023).
[4] G. Alva, Y. Lin, G. Fang, An overview of thermal energy storage sytems, Energy 144 (2018) 341–378.
[5] P. Arce, M. Medrano, A. Gil, E. Oró, L.F. Cabeza, Overview of thermal energy storage (TES) potential energy savings and climate change mitigation in Spain and Europe, Appl. Energy 88 (2011) 2764–2774.
[6] A. Alkhalidi, H. Al Khatba, M.K. Khawaja, Utilization of buildings' foundations for a seasonal thermal energy storage medium to meet space and water heat demands, Int. J. Photoenergy 2021 (2021) 6668079.
[7] I. Dincer, M.A. Rosen, Thermal energy storage systems and applications, John Wiley & Sons, Hoboken, NJ, USA, 2021.
[8] E. Borri, G. Zsembinszki, L.F. Cabeza, Recent developments of thermal energy storage applications in the built environment: A bibliometric analysis and systematic review, Appl. Therm. Eng. 189 (2021) 116666.
[9] P. Denholm, J.C. King, C.F. Kutcher, P.P. Wilson, Decarbonizing the electric sector: Combining renewable and nuclear energy using thermal storage, Energy Policy 44 (2012) 301–311.
[10] M. Papapetrou, G. Kosmadakis, A. Cipollina, U. La Commare, G. Micale, Industrial waste heat: Estimation of the technically available resource in the EU per industrial sector, temperature level and country, Appl. Therm. Eng. 138 (2018) 207–216.
[11] H. Mahon, D. O'Connor, D. Friedrich, B. Hughes, A review of thermal energy storage technologies for seasonal loops, Energy 239 (2022) 122207.
[12] D.P.M. Meena, M. Choudhary, Thermal energy storage in sensible materials: a review, Int. J. Adv. Res. Ideas Innov. Technol. 3 (2017) 607–613.
[13] International Renewable Energy Agency (IRENA), The Energy Technology Systems Analysis Programmes (ETSAP): Technology Brief E17, International Energy Agency, Paris, France, 2013, https://iea-etsap.org/E-TechDS/HIGHLIGHTS%20PDF/E17IR%20ThEnergy%20Stor_AH_Jan2013_final_GSOK%201.pdf. (Accessed 21 February 2023).
[14] S. Green, J. McLennan, P. Panja, K. Kitz, R. Allis, J. Moore, Geothermal battery energy storage. Renewable energy, Int. J. Adv. Res. Ideas Innov. Technol. 164 (2021) 777–790.
[15] F. Cheruy, J.L. Dufresne, S.A. Mesbah, J.Y. Grandpeix F. Wang, Role of soil thermal inertia in surface temperature and soil moisture-temperature feedback, J. Adv. Modelling Earth Syst. 9 (2017) 2906–2919.
[16] A.L. Reed, A.P. Novelli, K.L. Doran, S. Ge, N. Lu, J.S. McCartney, Solar district heating with underground thermal energy storage: Pathways to commercial viability in North America, Renew. Energy 126 (2018) 1–13.
[17] D. Mangold, O. Miedaner, E.P. Tziggili, T. Schmidt, M. Unterberger, B. Zeh, Technisch-wirtschaftliche analyse und Weiterentwicklung der solaren Langzeit-Wärmespeicherung. Schlussbericht zum BMU-Forschungsvorhaben N, 329607, in: Technical report, Bundesministerium für Umwelt, Naturschutz, nukleare Sicherheit und Verbraucherschutz, Berlin, Germany, 2012.
[18] S. Gehlin, Borehole thermal energy storage, Adv. Ground-Source Heat Pump Syst. (2016) 295–327.
[19] H.S. Lim, J.S. Ok, J.S. Park, S.J. Lee, S.W. Karng, Y.T. Kang, Efficiency improvement of energy storage and release by the inlet position control for seasonal thermal energy storage, Int. J. Heat Mass Transfer 151 (2020) 119435.
[20] C.A. Cruickshank, C. Baldwin, Sensible thermal energy storage: diurnal and seasonal, in: T.M. Letcher (Ed.), Storing Energy, Elsevier, New York, NY, USA, 2016, pp. 291–311.
[21] M. Reuß, The use of borehole thermal energy storage systems, in: In Advances in Thermal Energy Storage Systems, Woodhead Publishing, 2021, pp. 139–171.
[22] M.M.A. Khan, R. Saidur, F.A. Al-Sulaimana, A review for phase change materials (PCMs) in solar absorption refrigeration systems, Renew. Sustain. Energy Rev. 76 (2017) 105–137.
[23] L.T. Terziotti, M.L. Sweet, J.T. McLeskey Jr, Modeling seasonal solar thermal energy storage in a large urban residential building using TRNSYS 16, Energy Build. 45 (2012) 28–31.
[24] M. Diago, A.C. Iniesta, A. Soum-Glaude, N. Calvet, Characterization of desert sand to be used as a high-temperature thermal energy storage medium in particle solar receiver technology, Appl. Energy 216 (2018) 402–413.
[25] I. Beausoleil-Morrison, B. Kemery, A.D. Wills, C. Meister, Design and simulated performance of a solar-thermal system employing seasonal storage for providing the majority of space heating and domestic hot water heating needs to a single-family house in a cold climate, Sol. Energy 191 (2019) 57–69.
[26] J. Lu, G. He, F. Mao, Solar seasonal thermal energy storage for space heating in residential buildings: Optimization and comparison with an air-source heat pump, Energy Sources Part B Econ. Plan. Policy 15 (2020) 279–296.
[27] J. Formhals, F. Feike, H. Hemmatabady, B. Welsch, I. Sass, Strategies for a transition towards a solar district heating grid with integrated seasonal geothermal energy storage, Energy Sources Part B Econ. Plan. Policy 228 (2021) 120662.
[28] X. Zhou, Y. Xu, X. Zhang, D. Xu, Y. Linghu, H. Guo, Z. Wang, H. Chen, Large scale underground seasonal thermal energy storage in China, J. Energy Storage 33 (2021) 102026.
[29] H. Lund, S. Werner, R. Wiltshire, S. Svendsen, J.E. Thorsen, F. Hvelplund, B.V. Mathiesen, 4Th generation district heating (4GDH): Integrating smart thermal grids into future sustainable energy systems, Energy 68 (2014) 1–11.
[30] M. Reuß, R. Koenigsdorff, R. Zorn, J. Kuckelkorn, H. Steger, M. Pröll, P. Feuerstein, Qualitätssicherung bei Erdwärmesonden und Erdreichkollektoren, Abschlussbericht, Bundesministerium für Wirtschaft und Technologie (FKZ 0327453A), 2012.
[31] V.D.I. Guideline V.D.I. 4640, Thermal use of the underground, part 5: Thermal response test, 2019, Beuth-Verlag Berlin. https://www.vdi.de/richtlinien/details/vdi-4640-blatt-5-thermal-use-of-the-underground-thermal-response-test-trt. (Accessed 21 February 2023).
[32] Arquitectura Bioclimática y Frío Solar (ARFRISOL), Proyecto Singular Estratégico Ref. PS-120000–2005-1. Plan Nacional de Investigacióny Desarrollo 2004–2007, Ministry of Science and Innovation, Spain.
[33] M.J. Suárez, J.I. Prieto, E. Blanco, D. García, Tests of an absorption cooling machine at the gijón solar cooling laboratory, Energies 13 (2020) 3962.
[34] Eficiencia energética a través de la Rehabilitación, el Sol y la Geotermia en Asturias. (REHABILITAGEOSOL), RTC-2016-5004-3, Ministry of Economy, Industry and Competetiveness, Spain.
[35] A. Meana-Fernández, M.J. Suárez-López, D. García-Menéndez, E. Blanco-Marigorta, J.-I. Prieto, Experimental analysis of the feasibility of using the ground as a temporary energy accumulator, in: Proceedings of 36th International Conference on Efficiency, Cost, Optimization, Simulation and Environmental Impact of Energy Systems (ECOS 2023). Las Palmas de Gran Canaria, 25-30 June 2023, 4, 2023, pp. 2080–2091.
[36] W.K. Pratt, Digital Image Processing, fourth ed., John Wiley & Sons, Hoboken, NJ, USA, 2007, pp. 30–35.
[37] Y.A. Çengel, A.J. Ghajar, Heat and Mass Transfer – Fundamentals & Applications, 5th ed., McGraw-Hill, New York, NY, USA, 2015, pp. 30–35.
[38] J.M. Ándujar Márquez, M.A. Martìnez Bohórquez, S. Gómez Melgar, Ground thermal diffusivity calculation by direct soil temperature measurement. Application to very low enthalpy geothermal energy systems, Sensors 16 (2016) 306.
[39] T. Arkhangelskaya, K. Lukyashchenko, Estimating soil thermal diffusivity at different water contents from easily available data on soil texture, bulk density, and organic carbon content, Biosyst. Eng. 168 (2018) 83–95.
[40] B. Tong, H. Xu, R. Horton, L. Bian, J. Guo, Determination of long-term soil apparent thermal diffusivity using near-surface soil temperature on the Tibetan plateau, Remote Sens. 14 (2022) 4238.
[41] Agencial Estatal de Meteorología de España, Datos abiertos, 2022, https://www.aemet.es/es/datos_abiertos. (Accessed 21 February 2023).
[42] O.T. Farouki, Thermal properties of soils, in: Technical report, Cold Regions Research and Engineering Lab, Hanover, NH, USA, 1982.
[43] V.N. Dimo, Physical properties and elements of the heat regime of permafrost meadow-forest soils, in: Technical report, Cold Regions Research and Engineering Lab, Delhi: Indian National Scientific Documentation Centre, 1969.
[44] A.V. Luikov, Heat and mass transfer in capillary porous bodies, Pergamon Press, New York, NY, USA, 1966.
[45] D.A. De Vries, Heat transfer in soils, in: D.A. De Vries, N.A. Afghan (Eds.), Heat and Mass Transfer in the Biosphere. 1. Transfer Processes in Plant Environment, John Wiley & Sons, Inc., Halsted Press, New York, NY, USA, 1974.